

THE FRACTAL DIMENSION OF PROJECTED CLOUDS

Néstor Sánchez,^{1,2} Emilio J. Alfaro,¹ and Enrique Pérez¹

ABSTRACT

The interstellar medium seems to have an underlying fractal structure which can be characterized through its fractal dimension. However, interstellar clouds are observed as projected two-dimensional images, and the projection of a tri-dimensional fractal distorts its measured properties. Here we use simulated fractal clouds to study the relationship between the tri-dimensional fractal dimension (D_f) of modeled clouds and the dimension resulting from their projected images. We analyze different fractal dimension estimators: the correlation and mass dimensions of the clouds, and the perimeter-based dimension of their boundaries (D_{per}). We find the functional forms relating D_f with the projected fractal dimensions, as well as the dependence on the image resolution, which allow to estimate the “real” D_f value of a cloud from its projection. The application of these results to Orion A indicates in a self-consistent way that $2.5 \lesssim D_f \lesssim 2.7$ for this molecular cloud, a value higher than the result $D_{per} + 1 \simeq 2.3$ some times assumed in literature for interstellar clouds.

Subject headings: ISM: structure — ISM: clouds — ISM: general

1. INTRODUCTION

Maps of nearby cloud complexes have shown that the gas and dust are organized into irregular hierarchical structures which seem similar to each other over a wide range of scales (Scalo 1990; Falgarone et al. 1992). This self-similarity has been interpreted as a signature of an underlying fractal geometry that may be related to the physical processes supporting the generation of structures in the interstellar medium. The origin of this fractal-like structure seems to be turbulence (Falgarone & Phillips 1990; Kritsuk & Norman 2004; Padoan et al. 2004), although self-gravity could also play an important role (de Vega et al. 1996). A fractal

¹Instituto de Astrofísica de Andalucía, CSIC, Apdo. 3004, E-18080, Granada, Spain; nestor@iaa.es, emilio@iaa.es, eperez@iaa.es.

²Departamento de Física, Universidad del Zulia, Maracaibo, Venezuela.

structure for the interstellar medium is consistent with many observed features, including the cloud size and cloud mass distribution functions (Elmegreen & Falgarone 1996), the properties of the intercloud medium (Elmegreen 1997a), and even the stellar initial mass function (Larson 1992; Elmegreen 1997b, 2002).

Therefore, it is important to measure the degree of fractality and/or complexity of the ISM. There are several ways this can be done, such as structure tree methods (Houllahan & Scalo 1992), delta variance techniques (Stutzki et al. 1998), principal components analysis (Ghazzali et al. 1999), multifractal analysis (Chappell & Scalo 2001), metric space techniques (Khalil et al. 2004), etc. A simple method consists of calculating the fractal dimension characterizing structures in the ISM, but it has to be mentioned that quantifying the fractal dimension of an object is generally not sufficient to characterize it, because objects with different morphological properties could have the same fractal dimension (Mandelbrot 1983). In spite of this a number of studies have been done to estimate the fractal dimension of interstellar clouds. Most of these studies use the so-called perimeter-area method: if the isocontours exhibit a power-law perimeter-area relation with a noninteger exponent over certain range of scales, this exponent may be interpreted in terms of a fractal dimension (D_{per}) that characterizes the manner these curves fill space (Mandelbrot 1983). This method was used by Beech (1987) on a group of selected dark clouds to estimate a fractal dimension of 1.4, whereas Bazell & Desert (1988) calculated an average fractal dimension of 1.26 for cirrus regions discovered by IRAS. Dickman et al. (1990) studied five different molecular cloud complexes (Chamaeleon, R CrA, ρ Oph, Taurus and the Lynds 134/183/1778 group) finding $1.17 \lesssim D_{per} \lesssim 1.28$. Also for the Taurus complex, Scalo (1990) found $D_{per} = 1.4$ and Falgarone et al. (1991) found $D_{per} = 1.36$ over a very wide range of sizes. Hetem & Lepine (1993) reported $1.3 \lesssim D_{per} \lesssim 1.52$ for the Chamaeleon complex with an average of 1.44, a value notoriously higher than the one of Dickman et al. (1990). Vogelaar & Wakker (1994) also estimate relatively high values for D_{per} which generally range between 1.35 and 1.5 for high-velocity clouds and IRAS cirrus.

The observational evidence can be summarized by saying that the boundaries of molecular clouds appear to be fractal curves with dimension $D_{per} \sim 1.35$ (or some value in the range $1.2 \lesssim D_{per} \lesssim 1.5$). But the clouds are necessarily recorded as two-dimensional images projected onto a plane perpendicular to the line-of-sight. The connection between D_{per} and the fractal dimension of the tri-dimensional clouds is still an open question. The fractal nature of the projected boundaries suggests that these clouds may have fractal surfaces with dimensions given by $D_{per} + 1$ (Mandelbrot 1983). Then, it is usually assumed that $D_{per} + 1 \simeq 2.35$ should be the fractal dimension of interstellar clouds (e.g. Beech 1992). However, although it is possible that much of their internal structure is directly reflected in surface features, there is not necessarily any simple relation between the fractal dimension of the surface of

a cloud and that of its internal structure. On the other hand, it has been proven that the intersection of a fractal with dimension D_f and a plane gives another fractal with dimension given by $D_f - 1$ (Mandelbrot 1983), but a projection is a totally different operation and the result $D_{pro} = D_f - 1$ does not have to be expected for the projected fractal dimension. In fact, if an object of fractal dimension D_f embedded in a tri-dimensional Euclidean space, is projected on a plane, it is possible to show that the projection has dimension $D_{pro} = D_f$ or $D_{pro} = 2$ depending on whether $D_f < 2$ or $D_f > 2$, respectively (Falconer 1990). Thus, the projection of a cloud with $D_f \simeq 2.35$ would give rise to a compact shadow that may not be a fractal, but we want to emphasize that the relationship between the fractal dimension of this projection and that of its boundary is not clearly established.

The purpose of this work is to investigate the relationship between the fractal dimension of a tri-dimensional cloud and the fractal dimension of its projection, both for the whole projected image and for its boundary. To do this we use artificial fractal clouds generated by using an algorithm which mimics in some way the hierarchical fragmentation process occurring in molecular cloud complexes. Our main goal is to estimate the real fractal dimension of interstellar clouds from observed images. In § 2, we explain the manner in which we simulate the clouds and, after a brief review on some definitions of fractal dimension, we calculate the fractal (correlation and mass) dimensions of the projected clouds. In § 3, we address the perimeter-area relation of the projected images and its dependence on the image resolution. This analysis is applied to the Orion A molecular cloud in § 4 and, finally, the main results are discussed in § 5.

2. FRACTAL DIMENSION OF SIMULATED CLOUDS

We first have to generate tri-dimensional fractal clouds. For convenience we use simple recursive construction rules based on the Soneira & Peebles (1978) method. Within a sphere of radius R we place randomly N spheres of radius R/L with $L > 1$, in each of these spheres we place again N smaller spheres with radius R/L^2 , and so on up to level H of hierarchy. The set of N^H points (actually little spherical particles of radius R/L^H) in the last level forms an object with fractal dimension given by $D_f = \log N / \log L$. Most simulations were made using $N = 3$ fragments in a total of $H = 9$ levels of hierarchy ($\sim 2 \times 10^4$ particles in the last level) with the fractal dimension in the range $1 < D_f < 3$. However, when the fractal dimension is too high ($D_f \gtrsim 2.6$) the filling factor tends to 1 and it becomes difficult

to place randomly the spheres through all the volume without them being superposed¹. In these cases we use $N = 8$ fragments in $H = 5$ levels ($\sim 3 \times 10^4$ particles) and each fragment is placed randomly *within* the available volume in the direction of each of the eight octants. This allows us to reach high fractal dimension values (and filling factors) easily. In any case, several tests showed that our results do not depend (at least within the error bars) on N and/or H (as long as we have a sufficiently high number of particles in the last level). In order to illustrate the appearance of the point distributions, Figure 1 shows examples of projections of tri-dimensional fractals generated by using $N = 3$, $H = 9$ and three different values of fractal dimension ($D_f = 1.5, 2.0$ and 2.5).

2.1. Fractal Dimension Estimation

In the following, we will focus our attention on the empirical determination of the fractal dimension both for the simulated clouds and for their two-dimensional projections. In general, a fractal can be defined as a set of points whose Hausdorff dimension D_H is strictly larger than its topological dimension D_T (Mandelbrot 1983). To estimate the Hausdorff dimension authors normally use working definitions which fit their method and needs, and thus there is not a unique definition of fractal dimension. In general, a fractal quantity is a number which is connected to some length l in a manner like $A \sim l^{D_A}$, where D_A would be the (constant) dimension associated to the quantity A . The most straightforward way to estimate the Hausdorff dimension of a fractal set is through the box-counting method, based on the fact that the number of boxes, $N(r)$, having side r needed to cover a fractal object varies as r^{-D_B} , being D_B an estimation of D_H (Mandelbrot 1983) which is called the “box-counting dimension” (or “capacity”). Then, if we cover the object with a grid and count the number $N(r)$ of occupied cells of size r , we can compute

$$D_B = - \lim_{r \rightarrow 0} \frac{\log N(r)}{\log r} . \quad (1)$$

In practice D_B corresponds with the slope of the best fit in a $\log N - \log r$ plot, but obviously the range where this scale law is valid in real (finite) fractals is limited to the range between the smallest measurable region (the resolution) and the object size.

The major problem with the box-counting method is that it leads to imprecise results because of its sensitivity to, for example, the placement and orientation of the grid and

¹We avoid superposition because the tests made allowing superposition showed that the properties are modified in such a way that it appears a multifractal behavior and a unique fractal dimension can not be defined in a wide scale range

the range and sequence of values of box side length (Buczowski et al. 1998; Gonzato et al. 2000). A more useful method when dealing with a point distribution in space has been introduced by Grassberger & Procaccia (1983): given a set of N_p points with positions \mathbf{x} , one first computes the correlation integral $C(r)$ defined as

$$C(r) = \frac{2}{N_p(N_p - 1)} \sum_{1 \leq i < j \leq N_p} H(r - |\mathbf{x}_i - \mathbf{x}_j|) , \quad (2)$$

where H is the Heaviside step function. The summation counts the number of pairs for which the distance $|\mathbf{x}_i - \mathbf{x}_j|$ is less than r . For a fractal set the correlation integral scales at small r like r^{D_C} , being D_C the “correlation dimension” of the set, so that

$$D_C = \lim_{r \rightarrow 0} \frac{\log C(r)}{\log r} . \quad (3)$$

The dimension D_C can be identified with the slope of the log-log plot of $C(r)$ versus r , but usually this power-law behavior is valid only in a finite range. Different (larger) slopes can be observed at very small scales which are associated with random (experimental) errors, noise and with the lack of statistics of finite samples at very small scales; and there are deviations due to nonlinear effects for too large r values (Theiler 1987).

If one now regards the mass (number of particles) inside a sphere of radius r we can define the “mass dimension” (D_M) if the mass obeys the self-similar scaling relation (Mandelbrot 1983):

$$M(r) \sim r^{D_M} . \quad (4)$$

A simple algorithm to estimate D_M consists in generating a sequence of spheres with different radii, count the number of points inside each one, and calculate the slope in a $\log M$ versus $\log r$ plot. An obvious problem is where to place the spheres, because large fluctuations in M (lower values) can appear if the spheres lie by chance in or near the voids that exist in the distribution. To avoid this under-sampling problem we modified this algorithm in the following way. We choose randomly a position within the fractal cloud where we place spheres having progressively greater radii and we calculate the density (number of points per unit volume) in each case. Usually the density shows an absolute maximum corresponding to the sphere which gives a better sampling in that point, then we take only this sphere and reject all the other ones. This procedure is repeated many times at random positions through the whole fractal volume. Finally, if several spheres have the same radius we only consider the densest sphere (i.e., the “best” sampling) to calculate the mass corresponding to that radius value. With this strategy we improve the sampling taking the spheres containing more information throughout all the structure.

We have calculated the correlation and mass dimensions as a function of D_f for the simulated tri-dimensional fractal objects. Figure 2 shows the correlation integral as a function of distance (normalized to the maximum distance between two particles in the fractal r_{max}) for the same three fractal clouds shown in Figure 1. The solid lines do not show the best fit but the expected slope for each fractal dimension value D_f . As mentioned above, the correlation integral has a well-defined power-law dependence but over a limited range: for too high r values the slope becomes smaller as C approaches the asymptotical value $C = 1$, while for too small r values statistical fluctuations produce a steeper slope. This effect is more notorious for low fractal dimensions because the low filling factor values allow a bigger random component when placing the spheres in each level of hierarchy. Figure 3 shows the sphere mass $M(r)$ as a function of its radius for the same fractal clouds shown in Figure 1. Again, the lines show the expected (theoretical) slope value. In this case a low fractal dimension value ($D_f = 1.5$) shows more fluctuations because the fractal has more empty regions (see Figure 1) and there is a higher probability of underestimating the mass. Notwithstanding the errors being larger than with the correlation integral, a good estimation of the fractal dimension can be done with this method as it will be shown next. For a given (theoretical) fractal dimension D_f , we have calculated $C(r)$ and $M(r)$ for ten different random clouds and we have estimated the average correlation (D_C) and mass (D_M) dimensions. The results are plotted in Figure 4, where we can see that both D_C and D_M are very similar to the theoretical value D_f in the analyzed range ($1 < D_f < 3$), although the error bars are higher for D_M mainly for very low D_f values where there are more empty spaces in the simulated clouds.

2.2. Projected Fractal Dimension

We are interested in knowing what happens with the estimated values of fractal dimensions when the measurements are made on the two-dimensional projected images of the fractal clouds. It has been proven analytically that the projection of a fractal with tri-dimensional dimension D_f yields a projected dimension given by (Falconer 1990; Hunt & Kaloshin 1997):

$$D_{pro} = \min\{2, D_f\} . \quad (5)$$

Thus, D_f and D_{pro} are equal if $D_f < 2$ and $D_{pro} = 2$ if $D_f > 2$ (in this last case it would not be possible to estimate D_f from the projected image). However, equation (5) was deduced for indefinitely extensive (mathematical) fractals and its validity for real finite fractals with certain random component is not obvious. At least for random fractal aggregates the equation (5) can not be applied (Nelson et al. 1990; Jullien et al. 1994; Maggi & Winterwerp 2004). We have made projections of the simulated clouds on random planes and we have

calculated the average correlation and mass dimensions for the resulting projections. An example is shown in Figure 5, where we have plotted the correlation integral for the original tri-dimensional fractal and for its two-dimensional projection using the cloud with dimension $D_f = 1.5$ shown in Figure 1. The line indicates the expected slope (1.5) for both the tri-dimensional and bi-dimensional fractals (according to eq. 5). For the assumed values of N , H and D_f the smallest possible distance between two particles in the simulated fractal is $r_{min} \sim 10^{-3}$, and all the distances smaller than r_{min} in the projected fractal arise from the random projection itself. Thus, for $r > r_{min}$ we find that the projected fractal has a slope in the log-log plot similar to (although a little smaller than) the expected one, but for $r < r_{min}$ the slope increases tending to ~ 2 (the value corresponding to a random distribution of particles on the plane). When estimating the fractal dimension of the projected fractals we have considered only distances greater than r_{min} . Figure 6 shows the measured correlation dimension ($D_{C,2D}$) and mass dimension ($D_{M,2D}$) for the projected clouds as a function of the tri-dimensional fractal dimension (D_f). Each point is the result of calculating the average of ten different realizations (random fractals) and the bars indicate the standard deviations. We can see that the calculated values are always below the theoretical result given by equation (5), except for very low ($D_f \sim 1$) or very high ($D_f \sim 3$) fractal dimension values. This result looks similar to the one of Maggi & Winterwerp (2004) obtained for the capacity dimension of projected fractal aggregates. Since $D_{C,2D}$ varies continuously with D_f , one might generally be able to extract the fractal dimension of a three-dimensional cloud by analyzing the correlation dimension of its projection, even when $D_f > 2$, but $D_{C,2D}$ changes too slowly with D_f (within the error bars) for $D_f \gtrsim 2.5$. In spite of this degeneration both $D_{C,2D}$ and $D_{M,2D}$ could be used for doing a rough estimation of the fractal dimension D_f .

3. PERIMETER-AREA RELATION

The fractal dimension of a bounding contour can be determined via the perimeter-area relation (Mandelbrot 1983). In a plane, the perimeter (P) and the area (A) are related by

$$P \sim A^{D_{per}/2}, \quad (6)$$

where the dimension D_{per} characterizes the degree of perimeter contortion. Objects with smoothly varying contours (e.g. circles) will have $D_{per} = 1$ (i.e. $P \sim A^{1/2}$), whereas extremely convoluted plane-filling contours will have $D_{per} = 2$ ($P \sim A$). Thus, the irregularity of a bounding contour is characterized by $1 \leq D_{per} \leq 2$. The same argument applies for three-dimensional surfaces but in this case the dimension is 2 for smooth surfaces tending toward 3 for a convoluted surface which fills the space. The contour of a projected object is a subset of its surface and the measure of the contour D_{per} is not related (at least in an obvious

way) to, for example, the capacity D_B . The perimeter segmentation reflects the roughness of the boundary while the capacity measures the space-filling ability. Both of them, however, give information on the fractal structure of the object.

We wish to investigate to which extent the information of the tri-dimensional structure can be found from the projected perimeter-based fractal dimension D_{per} . In order to do this we first generate two-dimensional images applying the following procedure: we project the simulated clouds on random planes, then we place grids with various pixel sizes (resolutions) whose “brightness” is assigned by counting the number of particles inside each pixel. We define the image “resolution” (N_{pix}) as the ratio between the maximum two-pixel distance in the image and the pixel size (i.e. the resolution is the maximum object size in pixel units). The calculation of D_{per} begins fixing a threshold brightness level n_{cri} and defining each “object” into the image as a set of connected pixels (having a side or a corner in common) whose brightness value is above n_{cri} . The area of each object is found by counting the total number of pixels and the perimeter is calculated by summing the lengths of the sides of pixels along the edge of the object². Then, we calculate the best linear fit in a $\log P - \log A$ plot using the objects measured for different brightness levels and the slope of this fit would be $D_{per}/2$. To increase considerably the number of data points in the linear fit we have taken ~ 20 brightness levels equally spaced between the minimum and the maximum brightness. If an object is relatively small (containing less than a few pixels) its perimeter is not well defined and the structural details will disappear, we therefore demanded that objects contain a minimum (~ 15) number of pixels. Of course, several variations of the above procedure are possible: the definition of connectivity for neighbouring pixels (4-connected or 8-connected), the way for calculating the perimeter (for example, the length of the diagonal could be considered for the pixels at corners instead of the sum of the two sides), to take (or not) into account the inner holes, or the minimum number of pixels that can constitute one object in the fit. It has been proven that the estimation of D_{per} depends very weakly on these criteria (Vogelaar & Wakker 1994). In any case we tested the influence of all these criteria and verified that the result were not affected as long as objects too little were not considered in the procedure.

Figure 7 shows the perimeter-area based dimension D_{per} as a function of resolution N_{pix} for different values of the cloud fractal dimension D_f (for clarity, only five values of D_f are shown). The bars indicate the standard deviations resulting from 10 different realizations for each D_f values, the mean errors of the best linear fits in the $\log P - \log A$ plots always were less than these error bars. The first feature we note is that D_{per} decreases as D_f increases.

²In this computation, we consider the sum of both the external and the internal perimeter, i.e. the perimeter of the internal voids are also computed

This is an expected result because bigger D_f values generate clouds with more round-shaped boundaries, otherwise when D_f decreases the clouds have more irregular boundaries, as it can be seen in Figure 1. For a given fractal dimension D_f there is a tendency of D_{per} to decrease as N_{pix} decreases, and this is because when the pixel size is bigger the details of the roughness of the boundary disappear and the objects tend to have smoother boundaries (and $D_{per} \rightarrow 1$). Moreover, a very low number of pixels (and consequently number of objects) and/or very low D_f values (i.e. very fragmented structures) increase errors notoriously. On the other hand, at relatively high resolution values D_{per} converges toward some value which we associate with the “real” D_{per} value resulting from the projection. The dependence of D_{per} on D_f can be seen more clearly in Figure 8 for different fixed resolutions (only a few N_{pix} values are shown for clarity, but for $N_{pix} \gtrsim 400$ the curves overlap each other within the error bars). In general D_{per} decreases (from ~ 2 to ~ 1) as D_f increases (from ~ 1 to ~ 3), as can be seen in Figure 8a, but as resolution decreases the curves move down mainly at relatively high D_f values. Figure 8b shows D_{per} in a smaller range of D_f values but using 50 different random clouds instead of 10, so that the random fluctuations become smoother (these data are also shown in Table 1). We can estimate that if the perimeter-area relation of interstellar clouds images yields $D_{per} \simeq 1.35$ (this value is indicated with a horizontal line in Figure 8b) then the fractal dimension of the tri-dimensional cloud should be some value in the range $2.5 \lesssim D_f \lesssim 2.7$. This is higher than the result $D_f \simeq 2.3$ that could be inferred when a relation of the form $D_f = D_{per} + 1$ is assumed.

4. APPLICATION TO ORION A MOLECULAR CLOUD

In this section we use the results obtained to estimate the fractal dimension of Orion A giant molecular cloud³. We use a ^{13}CO (1-0) integrated intensity map obtained from high-resolution observations (15” beam and 40” grid spacing) with the 45 m telescope of the Nobeyama Radio Observatory (Tatematsu et al. 1993). To calculate D_{per} we run exactly the same algorithm used in § 3 for simulated clouds. Figure 9 shows the perimeter-area log-log plot for Orion A (in pixel size units). Each point represents different objects (clumps) for different intensity thresholds and the line shows the best linear fit including all the points plotted. The resulting dimension (twice the slope) is $D_{per} = 1.32 \pm 0.02$, a value within the range of measured dimensions in the interstellar clouds. As concluded before for the simulated clouds, from Figure 8b (see also Table 1) one obtains that the tri-dimensional fractal dimension of Orion A should be around 2.6 – 2.7.

³It has to be mentioned that Orion A has a very elongated morphology, and the analysis presented applies, in principle, to homogeneous and isotropic fractals

In order to verify this result we have decreased the resolution of the Orion A image in successive steps, defining new larger pixels whose intensities are given by the total intensities of the neighbouring pixels. The left side panel in Figure 10 is an image with the original resolution given by Tatematsu et al. (1993) while in the right side panel the size of each pixel is ten times the original one. The comparison of these images shows clearly that progressively worse resolutions smooth the contours decreasing its degree of convolutedness, because the details blend with each other. Thus, D_{per} should decrease when the resolution is degraded beyond a critical value which depends on the fractal dimension (as shown in Figure 7). In each step we have estimated the resolution N_{pix} (number of pixels along the maximum distance) and we have repeated the calculation of the perimeter-based dimension D_{per} . The results are shown in Figure 11, where for comparison we have also plotted the calculated results for the clouds simulated with $D_f = 2.5, 2.6$ and 2.7 . The bars indicate the standard errors of the fits and, although they become relatively high at low resolutions, it is clear from this Figure that the way in which D_{per} depends on N_{pix} for Orion A is consistent with a fractal dimension in the range $2.5 \lesssim D_f \lesssim 2.7$. The dependence of D_{per} on N_{pix} could be a better method to estimate D_f than one single D_{per} measure, mainly for low resolution observations.

A final test we can do is to estimate the mass dimension of Orion A by placing cells of different side sizes (r) on the image and calculating the total intensity of the cells. We call this quantity the “mass” $M(r)$ assuming that the intensity of each pixel is proportional to the total column mass along the line-of-sight. We have used the same algorithm explained in § 2 to calculate the mass as a function of the cell size, doing random sampling of relatively dense regions on the Orion A image. We first generate ~ 5000 random positions along the rectangle of $\sim 1000 \times 1300$ pixels containing the Orion A image (see Figure 12). The positions located outside the image ($\sim 80\%$) are automatically rejected as well as those positions where no relative density maximum is found when increasing the size of the cells (see § 2). At the end of this procedure, only ~ 40 points remained available to be used in the calculation of the mass dimension. Open circles in Figure 12 indicate the position of the final sampling on the CO map of Orion A used to calculate $M(r)$. We see that the algorithm avoids to select low density regions where noise could introduce a higher error in the determination of the mass dimension. Figure 13 is the resulting plot of $M(r)$ versus r for the Orion A cloud. The slope of the best fit (1.82 ± 0.03) can be associated with the mass dimension of the projected image ($D_{M,2D}$) from which we can obtain, using the results shown in Figure 6, that the tri-dimensional cloud would have a fractal dimension of $D_f \simeq 2.5 - 2.7$. This result is in agreement with the one obtained above from the perimeter-area relation. We tested the reliability of this result varying the sampling (both changing and increasing the number of random positions on the image), and the estimated mass dimension remained unchanged

within the error bar resulting from the linear fit.

5. DISCUSSION AND CONCLUSIONS

In this work we have generated tri-dimensional clouds with given fractal dimensions (D_f) which we projected on a plane to calculate the fractal dimension of the projected image. *The main results derived from this empirical approach concern the functional forms relating the tri-dimensional and the projected fractal dimensions.* Both the correlation and the mass dimensions increase as D_f increases (Figure 6), but at least for the hierarchical, finite, random fractals we generated, the projected dimensions are always below the theoretical (expected) values given by equation (5). We also analyzed the perimeter-based fractal dimension (D_{per}) and its dependence on both D_f and the image resolution (N_{pix}). In general, D_{per} is a decreasing function of D_f , and it tends to decrease as N_{pix} decreases (Figures 7 and 8).

The results obtained with this method allow to estimate the “real” fractal dimension of a cloud from its projection using different fractal dimension estimators. The application to Orion A yields $D_{per} \simeq 1.32$ for this molecular cloud which implies, according to our results, a tri-dimensional fractal dimension around 2.6 – 2.7. Moreover, both the dependence of D_{per} on the resolution (Figure 11) and the projected mass dimension (Figure 13) confirm that $D_f \sim 2.6$ for Orion A. This value is clearly higher than the result $D_{per} + 1 \simeq 2.3$ some times assumed in literature for interstellar clouds (e.g. Beech 1992). Elmegreen & Falgarone (1996) concluded that the size and mass spectra of interstellar clouds can be the result of an ISM with *tri-dimensional* fractal dimension around 2.3, but Stutzki et al. (1998) have argued that this numerical agreement could be coincidental. In fact, Stutzki et al. (1998) used fractional Brownian motion structures to analyze the observed ISM properties concluding that the index of the power spectrum that best reproduces the observed characteristics is $\simeq 2.8$, which would correspond to a cloud surface fractal dimension of $D_{sur} \simeq 2.6$. Although this quantity is not necessarily equal to D_f , it is interesting to note the agreement with our results. The only result Stutzki et al. (1998) did not derive explicitly was $D_{per} = D_{sur} - 1 = 1.6$ for the corresponding perimeter-area dimension.

The relationship between D_f and the physical processes determining the ISM structure is still an open issue. Turbulent diffusion in an incompressible fluid gives $D_f \sim 2.3$ (Meneveau & Sreenivasan 1990) and this fact has been considered as evidence favoring the turbulent origin for the observed fractal structure (Elmegreen & Falgarone 1996). Our results seem to be in conflict with this interpretation, but one should not forget that ISM is a complex system where other effects (such as self-gravity, or compressibility) have to be taken into account. However, the results of the present study show a clear evidence favoring fractal

dimensions for interstellar clouds higher than the values more commonly assumed.

We want to thank Bruce Elmegreen for his valuable comments. We also thank the referee for his/her helpful comments and criticisms which improved this paper. N. S. would like to acknowledge the funding provided by CONDES (Universidad del Zulia), FONACIT (Venezuela), and the Secretaria de Estado de Universidades e Investigacion (Spain). E. J. A. acknowledges the financial support from MECyD through grants AYA-2001-1696 and AYA-2001-3939-C03-01, and from Consejeria de Educacion y Ciencia (Junta de Andalucia) through the group TIC 101. E.P. acknowledges financial support from spanish grants AYA-2001-3939-C03-01 and AYA-2001-2089.

REFERENCES

- Bazell, D. & Desert, F. X. 1988, *ApJ*, 333, 353
- Beech, M. 1987, *Ap&SS*, 133, 193
- Beech, M. 1992, *Ap&SS*, 192, 103
- Buczowski, S., Kyriacos, S., Nekka, F. & Cartilier, L. 1998, *Pattern Recognition*, 31, 411
- Chappell, D. & Scalo, J. 2001, *ApJ*, 551, 712
- de Vega, H. J., Sanchez, N. & Combes, F. 1996, *Nature*, 383, 56
- Dickman, R. L., Horvath, M. A. & Margulis, M. 1990, *ApJ*, 365, 586
- Elmegreen, B. G. 1997a, *ApJ*, 477, 196
- Elmegreen, B. G. 1997b, *ApJ*, 486, 944
- Elmegreen, B. G. 2002, *ApJ*, 564, 773
- Elmegreen, B. G. & Falgarone, E. 1996, *ApJ*, 471, 816
- Falconer, K. J. 1990, *Fractal Geometry: Mathematical Foundations and Applications* (London: Wiley & Sons)
- Falgarone, E. & Phillips, T. G. 1990, *ApJ*, 359, 344
- Falgarone, E., Phillips, T. G. & Walker, C. K. 1991, *ApJ*, 378, 186

- Falgarone, E., Puget, J.-L. & Perault, M. 1992, *A&A*, 257, 715
- Ghazzali, N., Joncas, G. & Jean, S. 1999, *ApJ*, 511, 242
- Gonzato, G., Mulargia, F. & Ciccotti, M. 2000, *Geophys. J. Int.*, 142, 108
- Grassberger, P. & Procaccia, I. 1983, *Phys. Rev. Lett.*, 50, 346
- Hetem, A. & Lepine, J. R. D. 1993, *A&A*, 270, 451
- Houllahan, P. & Scalo, J. 1992, *ApJ*, 393, 172
- Hunt, B. R. & Kaloshin, V. Y. 1997, *Nonlinearity*, 10, 1031
- Jullien, R., Tyhouy, R. & Ehrburger-Dolle, F. 1994, *Phys. Rev. E*, 50, 3878
- Khalil, A., Joncas, G. & Nekka, F. 2004, *ApJ*, 601, 352
- Kritsuk, A. G. & Norman, M. L. 2004, *ApJ*, 601, L55
- Larson, R. B. 1992, *MNRAS*, 256, 641
- Maggi, F. & Winterwerp, J. C. 2004, *Phys. Rev. E*, 69, 011405
- Mandelbrot, B. B. 1983, *The Fractal Geometry of Nature* (New York: Freeman)
- Meneveau, C., & Sreenivasan, K. R. 1990, *Phys. Rev. A*, 41, 2246
- Nelson, J. A., Crookes, R. J. & Simons, S. 1990, *J. Phys. D: Appl. Phys.*, 23, 465
- Padoan, P., Jimenez, R., Nordlund, A. & Boldyrev, S. 2004, *Phys. Rev. Lett.*, 92, 191102
- Scalo, J. 1990, in *Physical Processes in Fragmentation and Star Formation*, ed. R. Capuzzo-Dolcetta, C. Chiosi & A. Di Fazio (Dordrecht: Kluwer), 151
- Soneira, R. M., & Peebles, P. J. E. 1978, *AJ*, 83, 845
- Stutzki, J., Bensch, F., Heithausen, A., Ossenkopf, V. & Zielinsky, M. 1998, *A&A*, 336, 697
- Tatematsu, K. *et al.* 1993, *ApJ*, 404, 643
- Theiler, J. 1987, *Phys. Rev. A*, 36, 4456
- Vogelaar, M. G. R. & Wakker, B. P. 1994, *A&A*, 291, 557

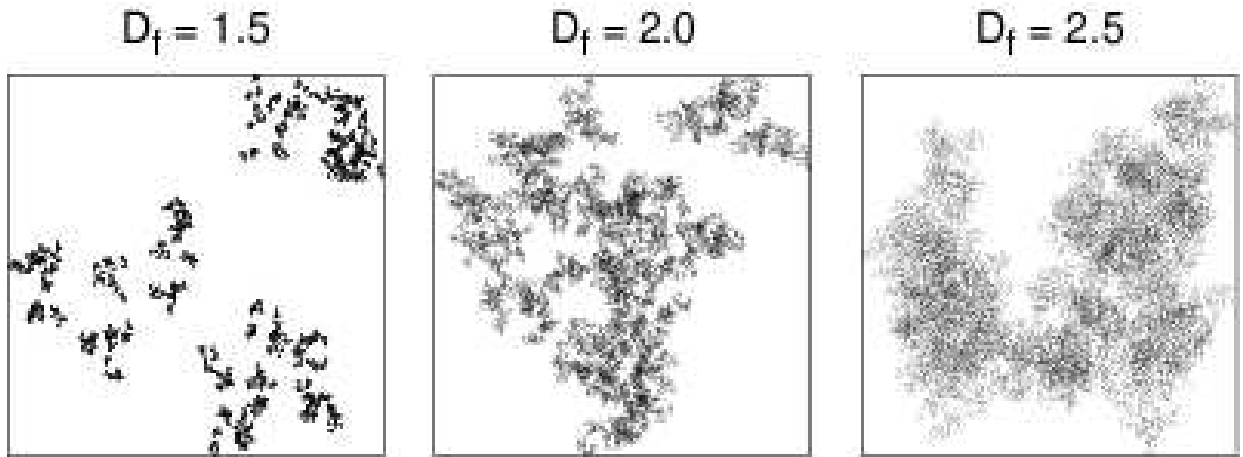


Fig. 1.— Examples of clouds simulated with $N = 3$ fragments per step in $H = 9$ levels of hierarchy for three different values of fractal dimension: 1.5, 2.0 and 2.5.

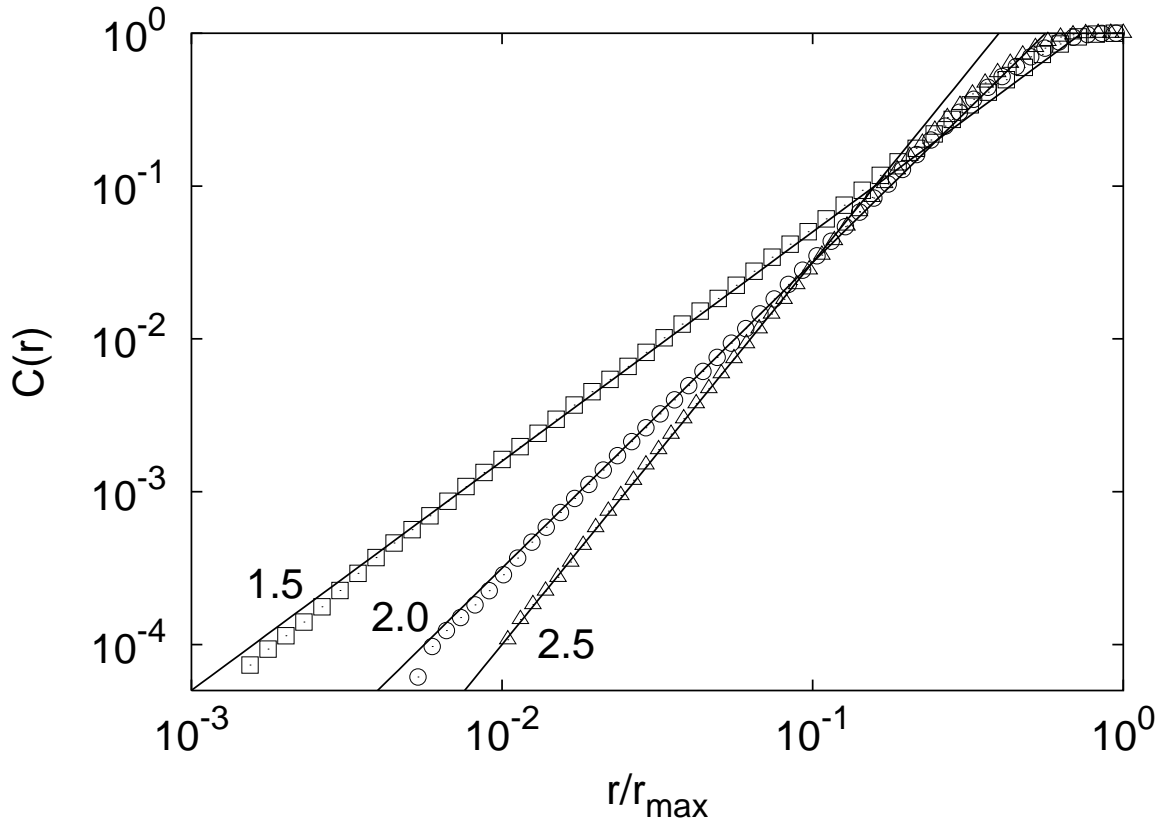


Fig. 2.— The correlation integral $C(r)$ for the three fractals shown in Figure 1: $D_f = 1.5$ (open squares), $D_f = 2.0$ (open circles) and $D_f = 2.5$ (open triangles). The lines show the expected slope for each fractal dimension value.

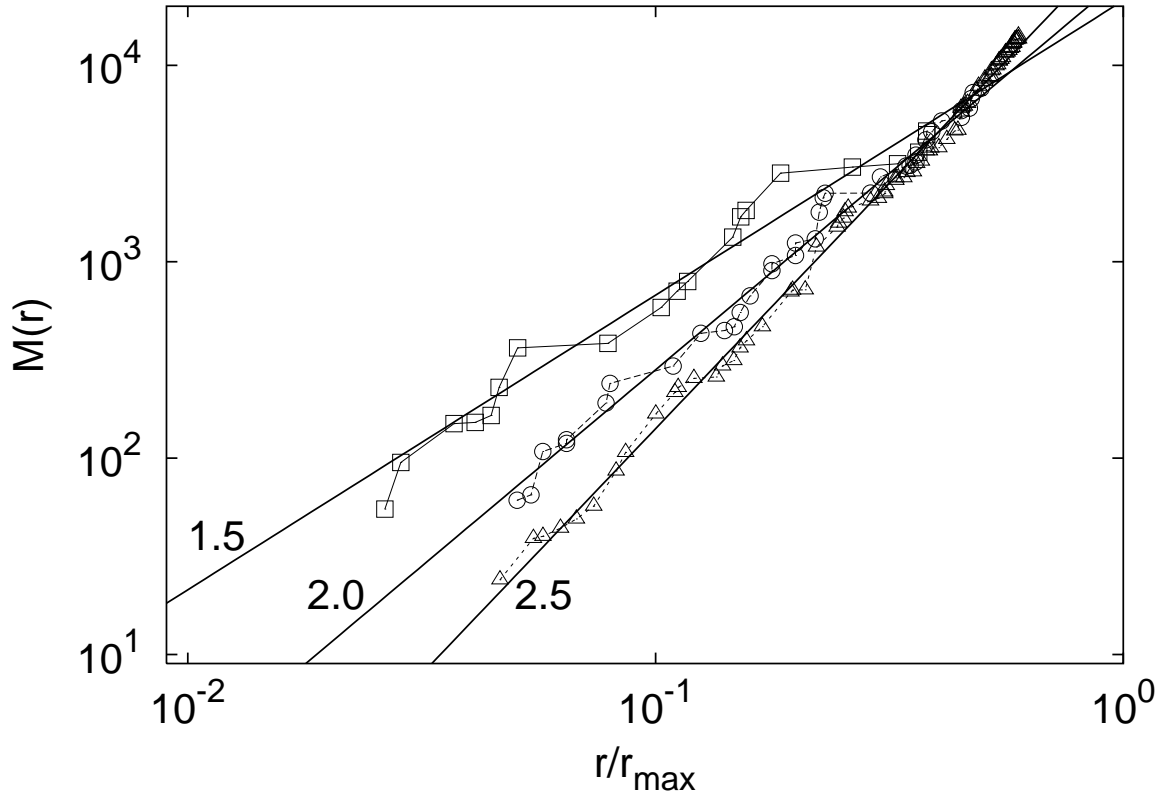


Fig. 3.— The mass $M(r)$ of the spheres of radius r for the three fractals shown in Figure 1: $D_f = 1.5$ (open squares), $D_f = 2.0$ (open circles) and $D_f = 2.5$ (open triangles). The lines show the expected slope for each fractal dimension value.

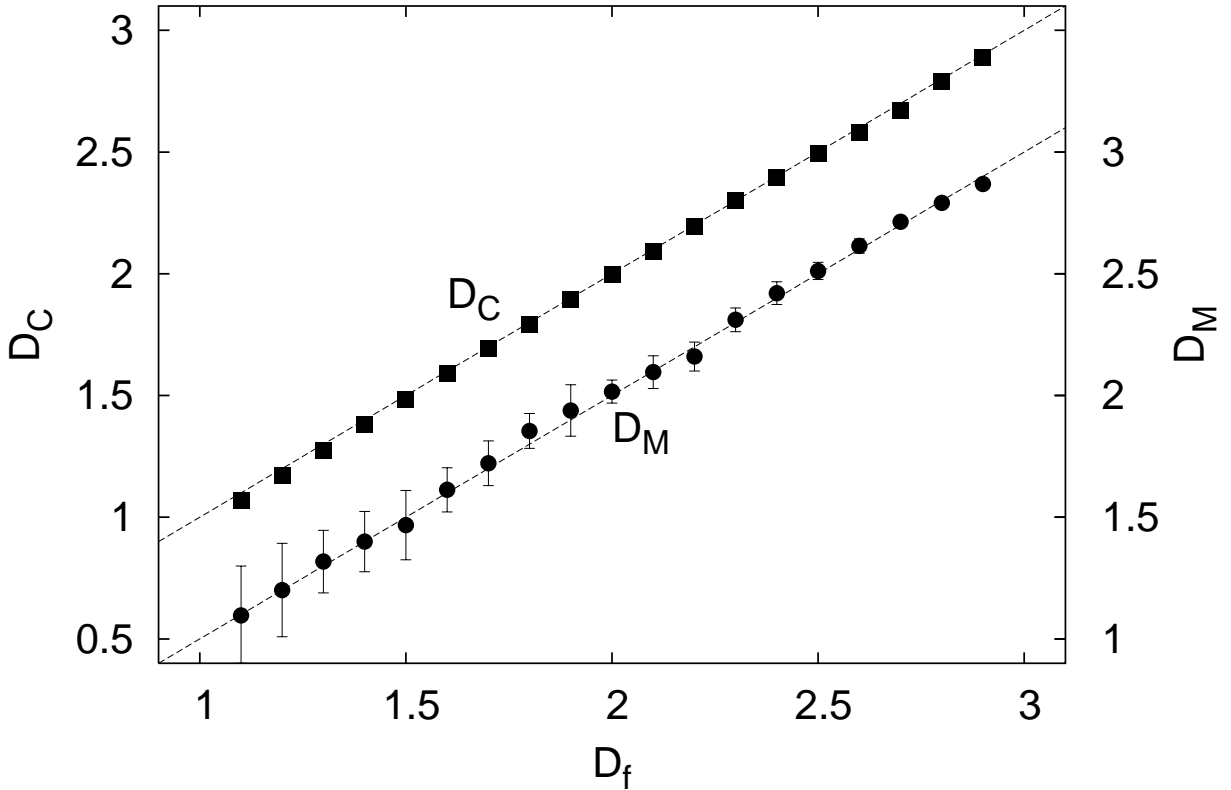


Fig. 4.— The calculated correlation dimension D_C (squares on the upper line and left side axis) and mass dimension D_M (circles on the lower line and right side axis) as a function of the fractal dimension D_f used to generate the cloud. Each point is the average of ten different realizations and the bars show the standard deviation. Dashed lines have slope unity.

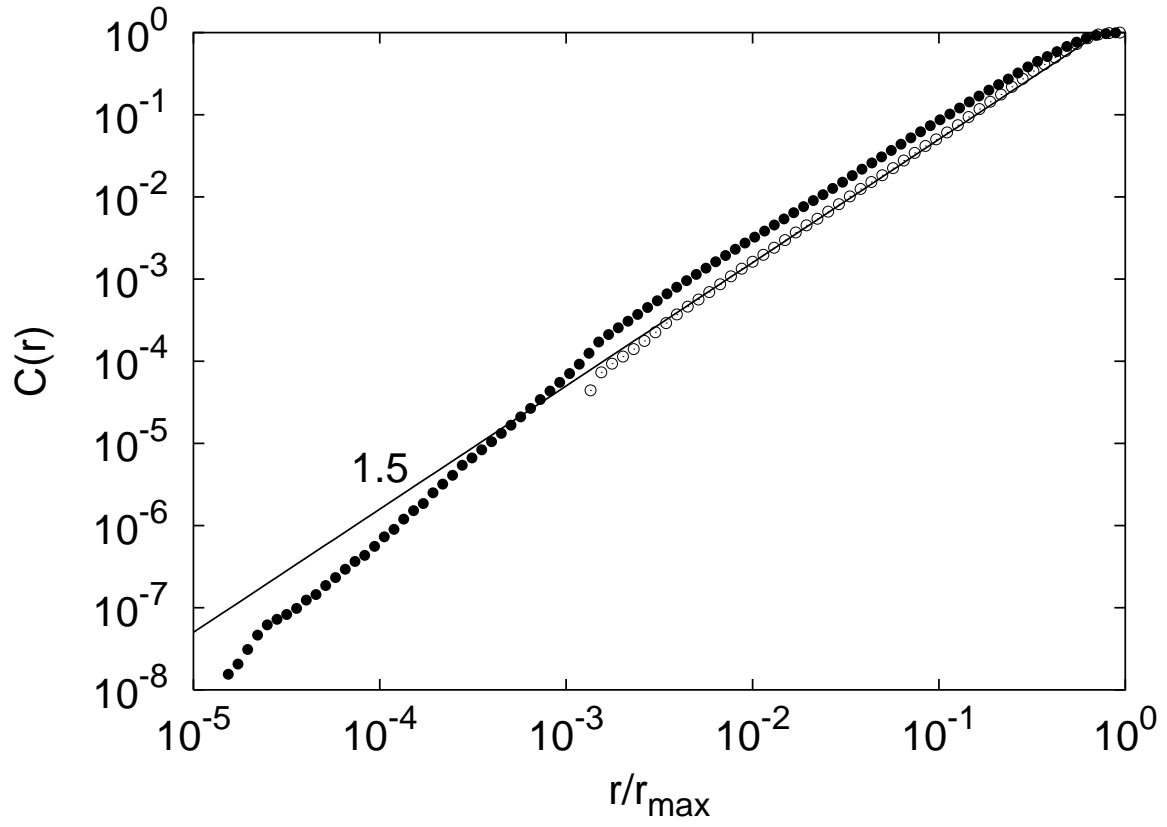


Fig. 5.— The correlation integral $C(r)$ for the fractal with $D_f = 1.5$ shown in Figure 1 (open circles) and for its projection (solid circles). The line shows the expected slope according to equation (5).

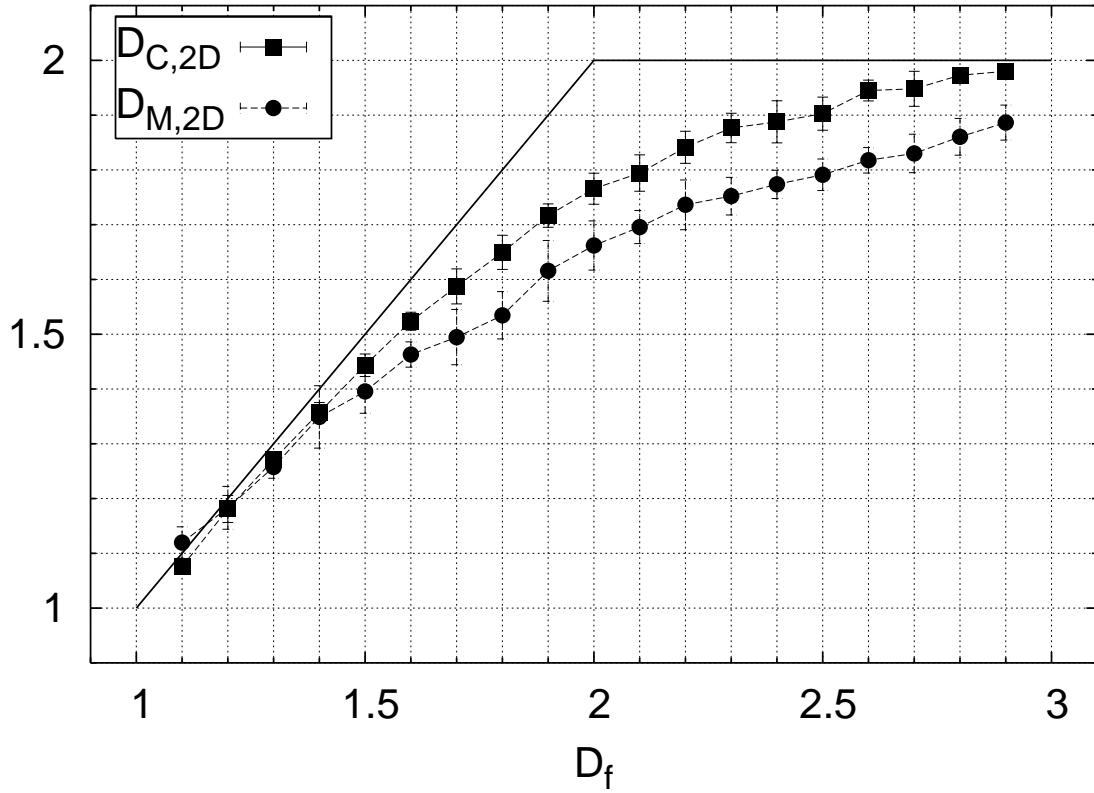


Fig. 6.— The average correlation dimension ($D_{C,2D}$, squares) and mass dimension ($D_{M,2D}$, circles) for the projected fractals as a function of the tri-dimensional fractal dimension (D_f). The solid line shows the theoretical result given by equation (5).

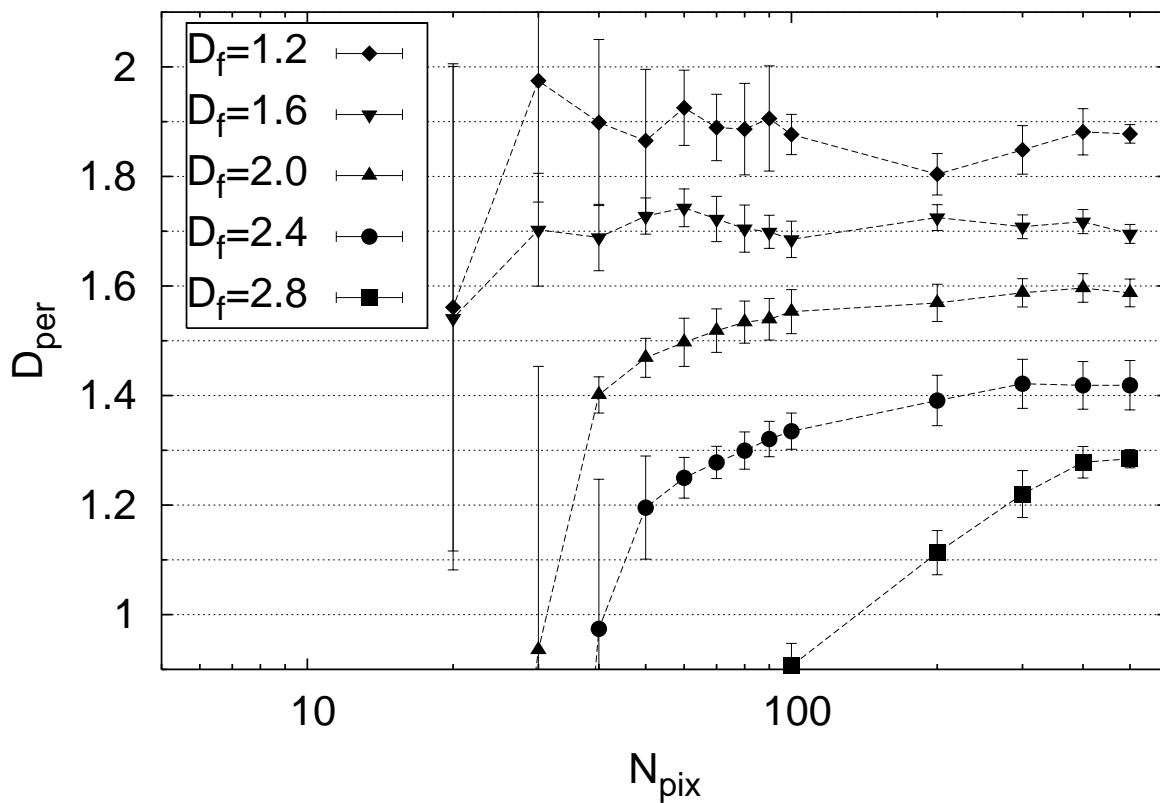


Fig. 7.— The perimeter-area based dimension D_{per} as a function of the projected image resolution N_{pix} for different cloud fractal dimensions: $D_f = 1.2$ (rhombuses), $D_f = 1.6$ (inverted triangles), $D_f = 2.0$ (triangles), $D_f = 2.4$ (circles), $D_f = 2.8$ (squares). The bars are the standard deviations resulting from ten different random realizations.

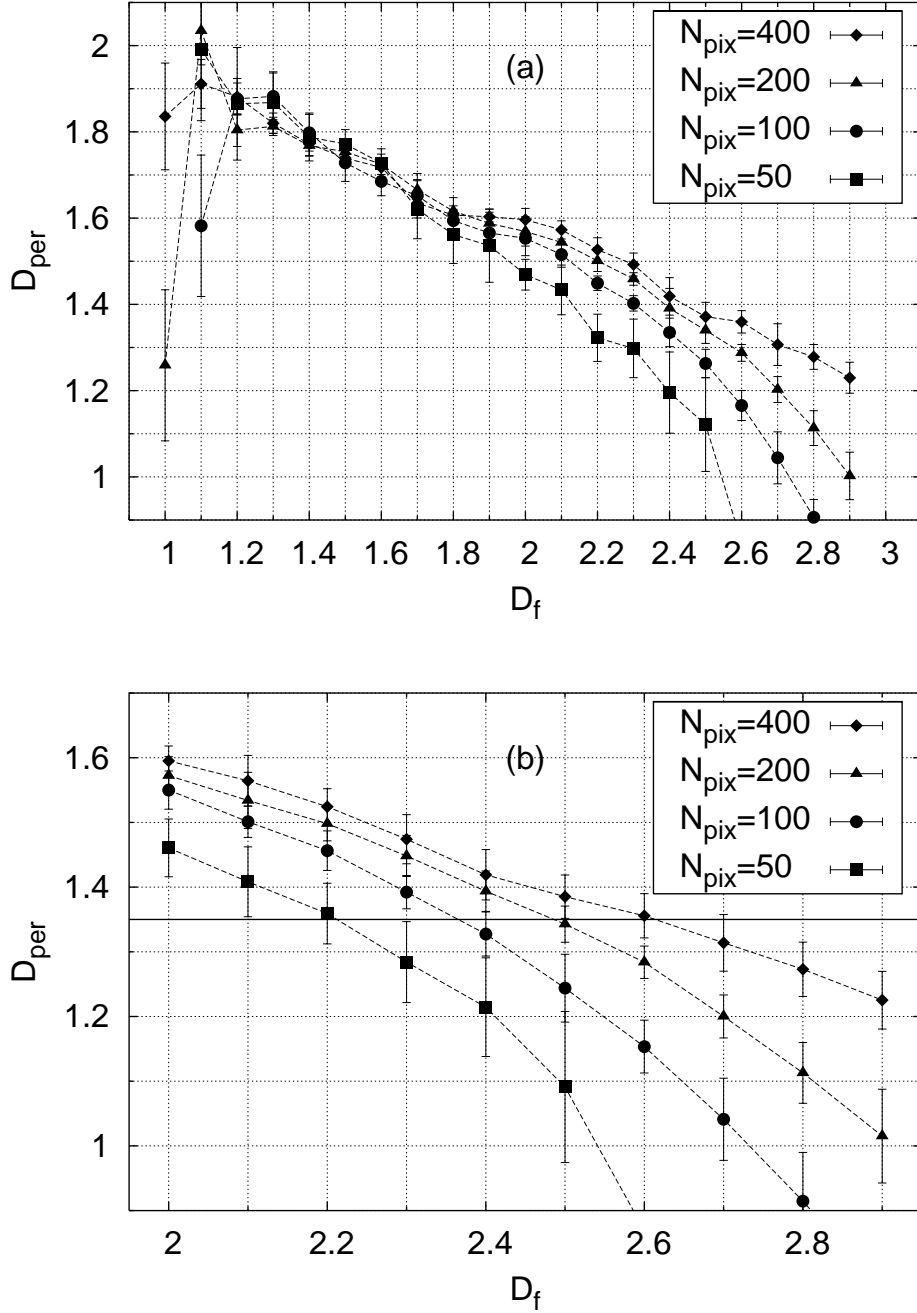


Fig. 8.— The perimeter-area based dimension D_{per} as a function of the cloud fractal dimension D_f for different resolutions: $N_{pix} = 400$ (rhombuses), $N_{pix} = 200$ (triangles), $N_{pix} = 100$ (circles) and $N_{pix} = 50$ (squares); calculated for (a) 10 different random clouds and (b) 50 random clouds but in a smaller range of D_f values. The horizontal solid line shows the value $D_{per} = 1.35$, and the bars are the standard deviations resulting from the different realizations.

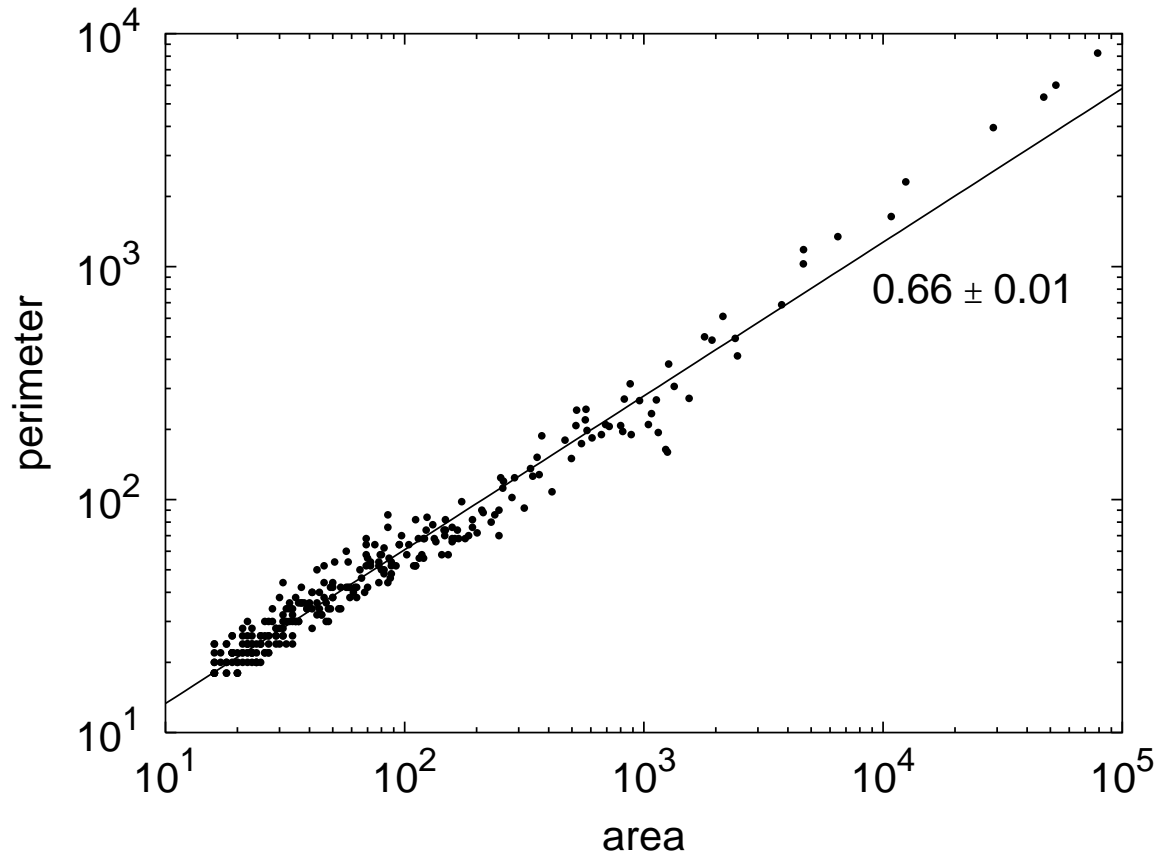


Fig. 9.— The perimeter as a function of the area (in pixel units) for objects in the Orion A region at different intensity levels. The line is the best linear fit for all the points shown.

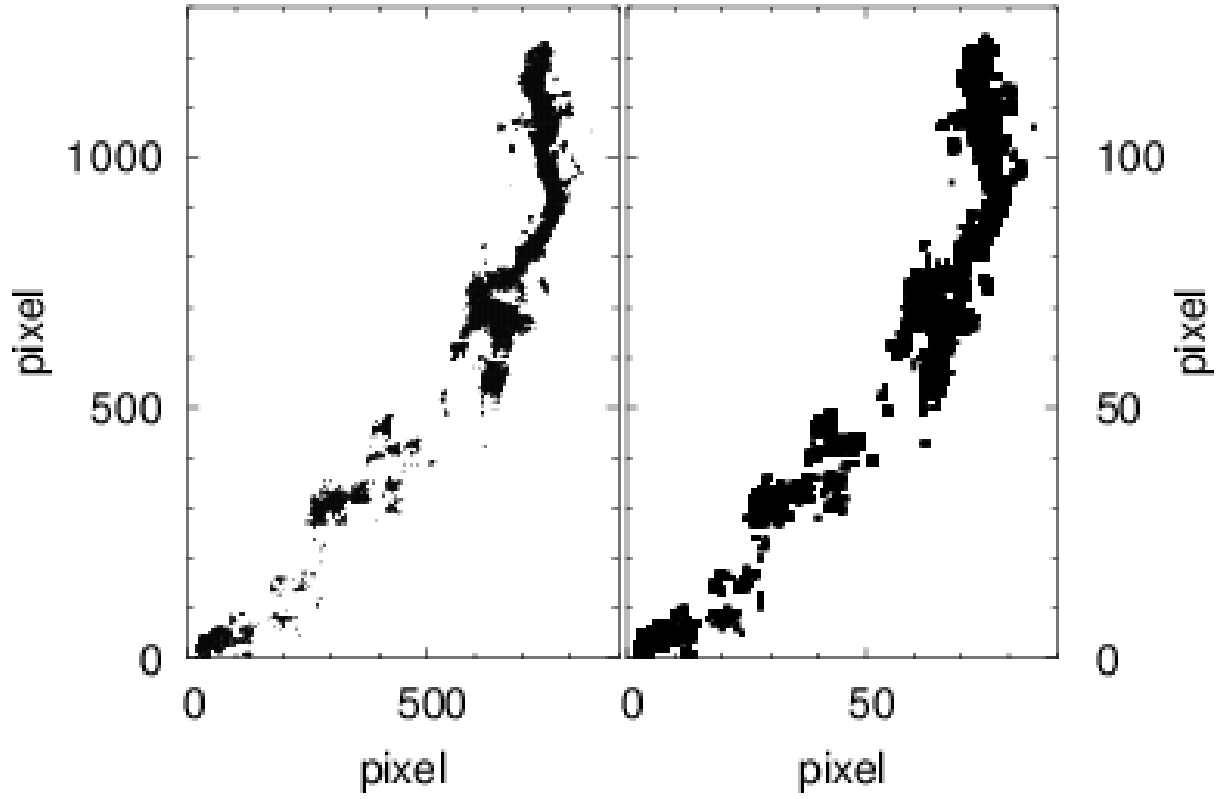


Fig. 10.— Two images of the Orion A molecular cloud at different resolutions. Left panel: the original resolution given by Tatematsu et al. (1993). Right panel: ten times the original pixel length.

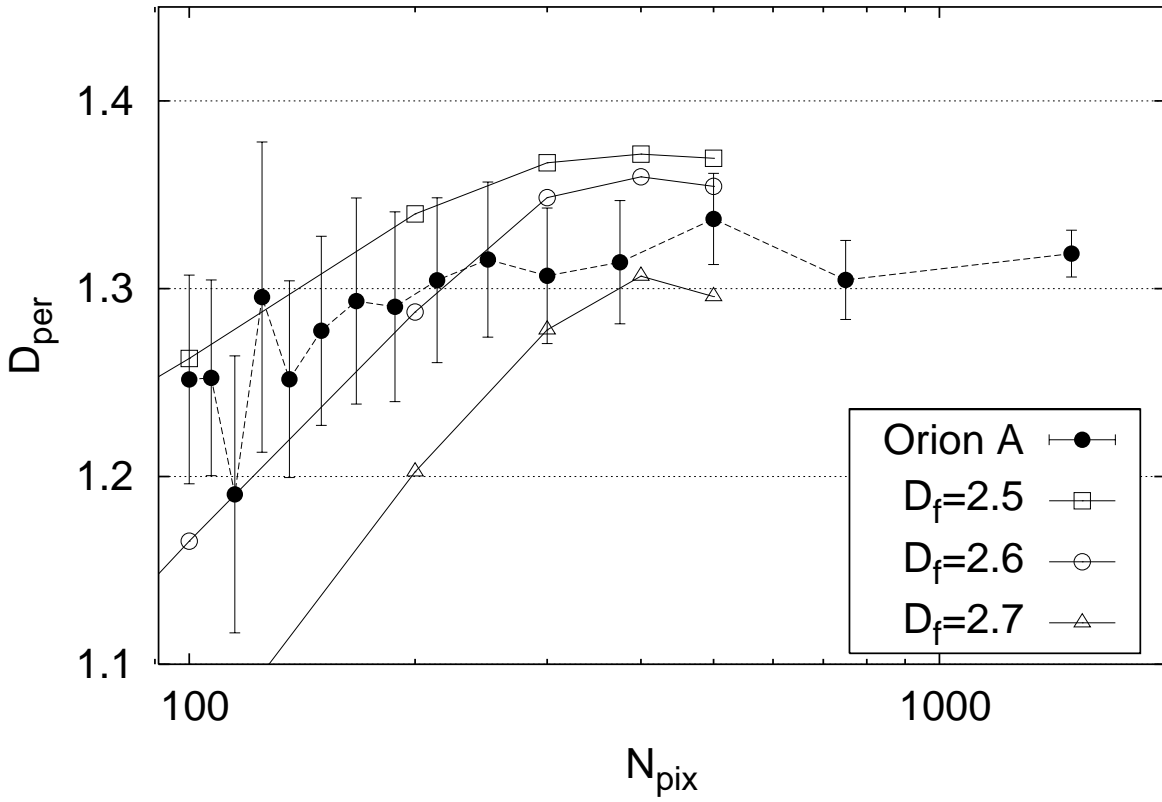


Fig. 11.— The perimeter-based dimension D_{per} as a function of the resolution N_{pix} for Orion A (solid circles) and for simulated clouds with $D_f = 2.5$ (open squares), $D_f = 2.6$ (open circles) and $D_f = 2.7$ (open triangles).

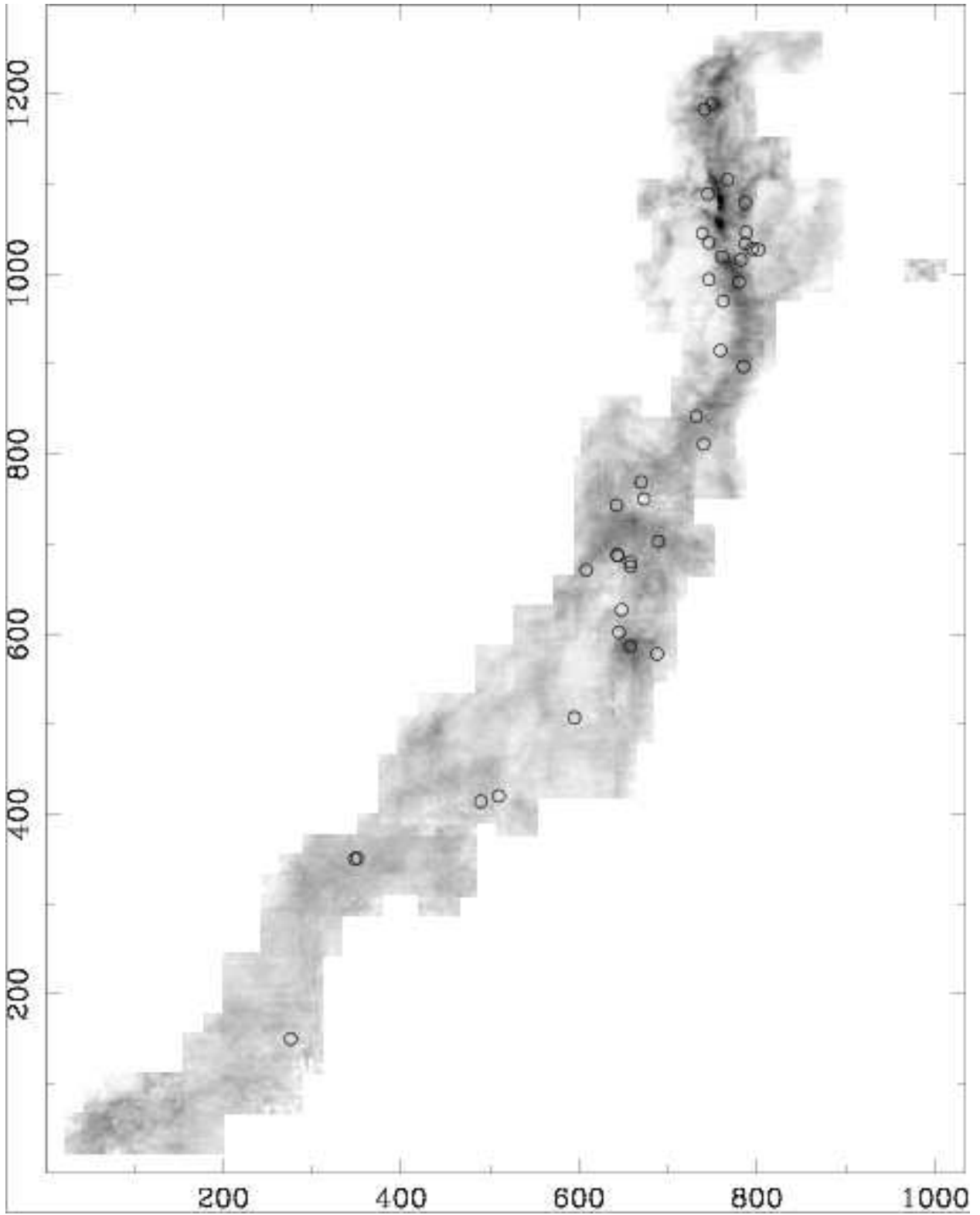


Fig. 12.— A ^{13}CO map of Orion A molecular cloud. The open circles indicate the positions of the sampling used to estimate the mass dimension of this image.

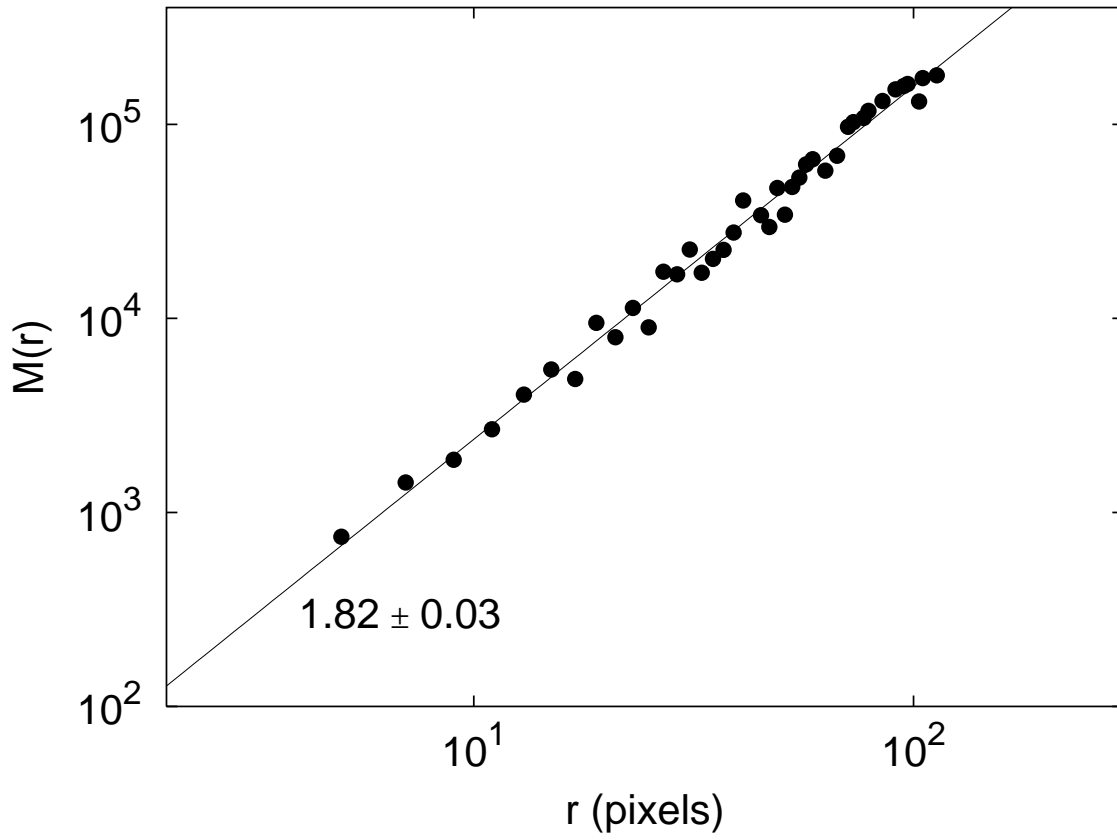


Fig. 13.— The “mass” $M(r)$ as a function of the cell size r for the Orion A molecular cloud. The solid line shows the best linear fit.

Table 1. Calculated perimeter-area based dimension

D_f	$N_{pix} = 50$	$N_{pix} = 100$	$N_{pix} = 200$	$N_{pix} = 400$
2.0	1.46±0.04	1.55±0.03	1.57±0.03	1.60±0.02
2.1	1.41±0.05	1.50±0.02	1.53±0.04	1.56±0.04
2.2	1.36±0.05	1.46±0.03	1.50±0.03	1.52±0.02
2.3	1.28±0.06	1.39±0.03	1.45±0.03	1.47±0.04
2.4	1.21±0.08	1.33±0.03	1.39±0.03	1.42±0.04
2.5	1.09±0.12	1.24±0.05	1.34±0.03	1.39±0.03
2.6	0.87±0.23	1.15±0.04	1.28±0.02	1.36±0.03
2.7	0.65±0.28	1.04±0.06	1.20±0.03	1.31±0.04
2.8	0.59±0.20	0.91±0.08	1.11±0.05	1.27±0.04
2.9	0.50±0.39	0.78±0.09	1.02±0.07	1.23±0.04